HHS Public Access

Author manuscript

Magn Reson Med. Author manuscript; available in PMC 2017 July 01.

Published in final edited form as:

Magn Reson Med. 2016 July ; 76(1): 237–247. doi:10.1002/mrm.25865.

Surface-to-volume ratio mapping of tumor microstructure using oscillating gradient diffusion weighted imaging

Olivier Reynaud[1,2,*], **Kerryanne Veronica Winters**[1,2], **Dung Minh Hoang**[1,2], **Youssef Zaim Wadghiri**[1,2], **Dmitry S Novikov**[1,2], and **Sungheon Gene Kim**[1,2]

[1]Center for Advanced Imaging Innovation and Research (CAI[2]R), New York, NY USA

[2]Bernard and Irene Schwartz Center for Biomedical Imaging, Department of Radiology, New York University School of Medicine, New York, NY USA

Abstract

Purpose—To disentangle the free diffusivity (D_0) and cellular membrane restrictions, via their surface-to-volume ratio (S/V), using the frequency-dependence of the diffusion coefficient $D(\omega)$, measured in brain tumors in the short diffusion-time regime using oscillating gradients (OGSE).

Methods—In vivo and ex vivo OGSE experiments were performed on mice bearing the GL261 murine glioma model (n=10) to identify the relevant time/frequency (t/ω) domain where $D(\omega)$ linearly decreases with $\omega^{-1/2}$. Parametric maps (S/V, D_0) are compared to conventional DWI metrics. The impact of frequency range and temperature (20°C vs. 37°C) on S/V and D_0 is investigated ex vivo.

Results—The validity of the short diffusion-time regime is demonstrated in vivo and ex vivo. Ex vivo measurements confirm that the purely geometric restrictions embodied in S/V are independent from temperature and frequency range, while the temperature dependence of the free diffusivity D_0 is similar to that of pure water.

Conclusion—Our results suggest that $D(\omega)$ in the short diffusion-time regime can be used to uncouple the purely geometric restriction effect, such as S/V, from the intrinsic medium diffusivity properties, and provides a non-empirical and objective way to interpret frequency/time-dependent diffusion changes in tumors in terms of objective biophysical tissue parameters.

Keywords

Surface-to-volume; Diffusion time-dependence; Oscillating Gradients Spin Echo; Mitra limit; Glioma; Restrictions

INTRODUCTION

The apparent diffusion coefficient (ADC) has been recognized in many studies as a promising potential imaging marker for tumor staging, treatment efficacy or cellularity (1–5). However, the use of a single ADC value as a quantitative metric for characterization of

*Address all correspondence to: Olivier Reynaud, PhD, Department of Radiology, NYU School of Medicine, 660 First avenue, 4th floor, New York, NY 10016. oli.reynaud@gmail.com; Tel: +001-212-263-0622.

various aspects of tumor microstructure is inherently limited, because the ADC can be affected by multiple factors, such as cell size, cell density, extracellular matrix, and diffusivities in different compartments.

Tissue complexity manifests itself in the non-Gaussian diffusion (6,7), characterized by (i) the presence of the higher-order terms in the cumulant expansion of MR signal S (8), $\ln(S) = -bD + (K/6)\cdot(bD)^2 +$ (such as the kurtosis term (9)), and (ii) the time-dependence of all the cumulants: $D(t)$, $K(t)$, … (10). Hence, tissue complexity can be probed in two complementary directions (11): (i) to quantify higher-order cumulants at a given diffusion time, by increasing the diffusion weighting parameter (b-value), and (ii) to probe the time dependence of the cumulants by varying the diffusion time t (equivalently, the frequency ω) at low b-value, as cumulants are the signal derivatives at $b \to 0$. In both directions, biophysical diffusion modeling in tissue microenvironment is required in order to quantify microstructural changes.

In this study, oscillating gradient spin echo (OGSE) acquisitions are used to explore the time-dependence of the diffusion coefficient — along direction (ii). Since the characteristic temporal scale, on which time-dependent metrics vary, provides a measure of the length scale for the relevant tissue microstructure, OGSE appears as a natural choice to focus on the smallest length scales (12).

While the long diffusion-time behavior of diffusion coefficient in a tissue depends on the structural disorder and packing correlations of tissue building blocks (13–15), the short-time limit is *universal*, being determined by the net amount of restrictions (such as cell walls). Porous media studies (16,17) demonstrated that the short-time behavior of the diffusion coefficient is given by an expansion in the powers of $\sqrt{t}$: $D(t) = D_0(1 - \mathrm{const}\cdot S/V\cdot\sqrt{D_0 t} + \cdots)$, where D_0 is the free diffusivity far from the restrictive walls (such as membranes), S/V is their surface-to-volume ratio, and the constant factor depends on the effective spatial dimensionality. Recently, the equivalent form of this regime was derived (18) for OGSE experiments (used to achieve the equivalent of short diffusion times): $D(\omega) = D_0(1 - c_d\cdot S/V\cdot\sqrt{D_0/\omega})$, where $c_d = 1/d\sqrt{2}$ in d dimensions. Reaching this asymptotic limit with OGSE would allow us to decouple the free diffusivity properties of the medium (D_0) from a purely geometrical tissue characteristic (S/V) that can be quantified non-invasively. Its inverse, V/S, gives an approximate estimate for the relevant cell size, and, more generally, a characteristic length scale for the separation between the membranes restricting the water molecules.

For packed beads, the S/V values estimated from OGSE experiments matched well with those predicted from a Monte Carlo simulation (19). Furthermore, S/V and D_0 values measured in synchronized cells were shown to be significantly different between cell cycle phases (20). Alternatively, recent works (21,22) attempted to describe time-dependent diffusion inside the mouse brain using an empirical parameter, Δ_fADC, representing the slope of the $D(\omega)$ variation with oscillation frequency. This approach was used for identifying various cell layers inside cortical areas (21), and for assessing treatment efficacy in a mouse glioma model (22). Despite the potential of the S/V–based approach to quantify

the typical restriction scale inside the tissue of interest (i.e. $S/V = 6/L$ for a cubic lattice with lattice constant L), there is still a paucity of studies on the S/V in tumors such that the predictive value of S/V parameter in cancer biology and imaging is not well understood to date.

In this study, we investigated whether the very short diffusion time regime, where the linear relationship between $D(\omega)$ and $t^{1/2} \sim \omega^{-1/2}$ holds, is reached in a mouse glioma model when using DWI-OGSE sequences in the range [65–225] Hz on a preclinical MRI scanner. We compared S/V and D_0 with conventional diffusion metrics from pulsed gradient spin echo (PGSE) and OGSE experiments. In addition, ex vivo DWI experiments were performed using a histology coil (23) to study the impact of temperature on D_0 and S/V. Combined together, both in vivo and ex vivo data were used to assess the consistency of diffusion parameters measured in the short diffusion time regime.

METHODS

MRI experiments were performed on a 7T Biospec micro-MRI system (Bruker Biospin MRI, Ettlingen, Germany) equipped with a Bruker BGA-9S gradient coil (75 G/cm gradient strength). All mice were treated in strict accordance with the National Institutes of Health Guide for the Care and Use of Laboratory Animals, and the experimental procedures were performed in accordance with the Institutional Animal Care and Use Committee at the New York University School of Medicine.

Animal protocol

GL261 intracranial cell implantation—Six- to eight-week-old female C57BL/6 mice (n=10) were anesthetized using 3% isoflurane in air. After induction, each subject was placed inside a stereotaxic frame. Anesthesia was maintained using 1.5% isoflurane in air. A small incision was made on the shaved head, and a small hole drilled in the skull (1.5/5.0 mm lateral/anterior to the bregma) to allow for the tumor cell injection. For each animal, 10^6 GL261 cells, suspended in 5 μL phosphate buffered saline (PBS), were injected into the subcortex (2.5 mm depth) using a Hamilton syringe (1 μL/min). After injection, the syringe was slowly removed (0.2 μm/min), the skull skin sutured and the animals carefully monitored until regaining consciousness.

In vivo imaging protocol—Mice were scanned once between day 14 and 28 after tumor implantation. Anesthesia was induced using 3% isoflurane in air. Animals were imaged using an in-house built quadrature Litz coil. Respiration and temperature were closely monitored and kept stable (60±10 bpm and T=35±1°C) throughout the entire MR session while general anesthesia was maintained (1.5% isoflurane in air). In vivo DWI consisted of OGSE and PGSE measurements, probing four diffusion times = 6/9/16/31 ms for PGSE, and ten oscillation frequencies in the range [65–225] Hz for the fast-ramp cosinusoidal OGSE (24) (number of oscillations $1 \leq N \leq 5$, see parameters in supporting Table S1). For the oscillating waveform, balanced ramps working near maximum slew-rate ($\text{relative slew-rate} = \sqrt{2}/2$, ramp duration 380 μs) (25) were used in order to remove potential DC components in the power spectrum. Pilot studies (Fig. 1A) revealed mono-

exponential signal behavior, negligible Intra-Voxel Incoherent Motion effects, and isotropic diffusion in the tumor for b<0.4 ms/μm^2 (=400 s/mm^2). As a result, diffusion-weighting gradients were only applied in one direction (1/1/1), using b=[0,0.2,0.4] ms/μm^2. Scans were centered on a single slice at the tumor center. The Spin-Echo EPI parameters were: TR/TE = 3000/70 ms, Bandwidth 300 kHz, 1 readout segment, number of averages NA=20, number of repetitions NR=2, pixel resolution 0.25×0.25×1.5 mm, matrix 80×80, TA = 6 min, total scan time 84 min. Diffusion times and oscillation frequencies were randomly sampled during the session. The whole series was repeated twice to monitor any changes due to temperature/motion.

Ex vivo sample preparation—After in vivo imaging, mice were anesthetized (ketamine/xylazine, intraperitoneal injection, 150/10 mg/kg) and transcardially perfused with PBS followed by 4% Paraformaldehyde (PFA). The extracted brain was immersed in 4% PFA overnight (4°C), then washed twice with PBS for 30 min intervals. Brain samples were cryoprotected in a series of sucrose gradients (15–30%) prior to embedding in optimal-compound temperature media and storage (−80°C). Axial sections were alternatively made with 5 μm thickness for immunohistochemical staining of GLUT1/Hematoxylin and 100 μm for ex vivo MR imaging. 100 μm thick slices were stored in 4% PFA (4°C).

Prior to ex vivo imaging, a 100 μm brain section was rehydrated for 2 hours in degassed PBS to avoid formation of microscopic air bubbles. It was then sealed between two coverslips to prevent tissue dehydration during MR acquisition. As in (23), Fomblin (Solvay Solexis Inc., Thorofare, NJ) was used as a hydrophobic sealant to contain the water within the tissue and fill the empty space between the two coverslips which were then glued together.

Ex vivo MR coil and DWI protocol—All ex vivo scans were performed with a dual-coverslip histology coil (Fig. 3C–D). Dedicated to thin samples, this coil provided a 6.7 fold increase in signal-to-noise (SNR) compared to commercial head mouse probes, while maintaining a very homogeneous transmit field all around the sample (23).

Each sample placed in the histology coil was carefully positioned in the horizontal plane and kept at room temperature, unless specified otherwise when investigating temperature. The diffusion-weighting direction was set in the horizontal plane to minimize any coverslip-induced restriction effect and eddy currents introduced by the strong diffusion gradients along the Left-Right direction at high frequencies (f_{OGSE}>160 Hz). The ex vivo MR protocol was adjusted as follows: NA=40, NR=6, and total acquisition time 11 hours.

Additional tests were performed on separate dates to study the impact of temperature and frequency range on D_0 and S/V. Samples (n=10) were first scanned at room temperature (NA=20, NR=2, TA=84 min). The sample temperature was then raised to and stabilized at 37±1°C using a regulated air heater system before DWI scans were repeated.

Data analysis

Theory—When the mean displacement is negligible compared to the characteristic size of the geometrical restrictions, we can represent all molecules by two populations: unrestricted (with volume fraction f_1, diffusing freely with diffusivity $D_1 = D_0$), and restricted (within the

diffusion length scale $\sim\sqrt{D_0 t}$ from the walls, with volume fraction $f_2 = 1 - f_1 \ll 1$ and a highly restricted diffusion coefficient $D_2 < D_0$). The overall diffusion coefficient, $D=\lim_{b\to 0}(-\mathrm{d}\ln S/\mathrm{d}b)$, defined by the first order term of the cumulant expansion (cf. introduction), is the weighted average, $D(t) = f_1 D_1 + f_2 D_2$, for a two-component system. The Mitra limit follows after estimating the restricted volume fraction as a volume of the thin molecular layer surrounding the walls: $f_2(t)\sim(S/V)\cdot\sqrt{D_0 t}$. The diffusion time (or oscillation frequency) domain in which the diffusion coefficient varies linearly with $t^{1/2}$ (equivalently, $\omega^{-1/2}$) will be referred to as the Mitra regime throughout this study, and it will be used to decouple the purely geometrical restriction measure (S/V) from the intrinsic diffusive properties of the medium (D_0).

The analytical expression of the OGSE-measured diffusion coefficient $D(\omega)$ was derived in the Mitra regime for a large number of oscillations ($N \gg 1$) (18). For a cosinusoidal gradient waveform and $N\sim1$, the coefficient $c(N)=\{4\pi N\cdot C(2\sqrt{N})+3\cdot S(2\sqrt{N})\}/(2\pi N)$ (where $C(x)$ and $S(x)$ are the Fresnel functions), modifies the prefactor in front of the S/V term (26), such that

$$D(\omega)=D_0(1-c(N)\cdot c_d\cdot S/V\cdot\sqrt{D_0/\omega}),\quad c_d=1/3\sqrt{2} \qquad [1]$$

for isotropic diffusion in $d=3$ dimensions relevant for glioma in the gray matter. Here ω is the oscillation frequency ($\omega = 2\pi f_{OGSE}$), and $c(N)$ monotonically decreases with N, approaching its large-N limit $c(\infty) = 1$ quite fast, as $N^{-3/2}$, with $c(1{:}5) =$ [1.14/1.08/1.06/1.05/1.04].

The validity of the Mitra regime was assessed in terms of how well the above functional form of the frequency describes the measured $D(\omega)$ by using the coefficient of determination R^2.

The impact of the correction factor $c(N)$ on the overall coefficient of determination was small for the range of N and ω used in this study (Fig. 1B, representative tumor, R^2=0.96 ($c(N)$, dotted line) vs. R^2=0.95 without the correction (c=1, dashed line)). However, since $D(\omega)$ varies linearly with $c(N)/\sqrt{\omega}$ according to Eq. [1], failure to account for the proper prefactor results in a nonnegligible S/V overestimation (Fig. 1B, 20%). Hence, $c(N)$ was always accounted for when calculating S/V, D_0 and R^2. Plots of $D(\omega)$ versus $\omega^{-1/2}$ were only used for visualization purposes, as in Fig. 2–3.

The coefficient of determination R^2 was calculated (a) on the average signal inside the tumor Region of Interest (ROI) (n=10), (b) voxel-by-voxel (n=1494) in the tumor ROI, and (c) voxel-by-voxel after spatial smoothing of the raw MR dataset (3×3 square kernel). This analysis was carried out with both in vivo and ex vivo data, in order to determine which conditions are better suited to the characterization of the tumor micro-environment via Eq. [1].

Comparison with empirical parameter, the slope Δ_fADC

For comparison, the $D(\omega)$ data were averaged inside the tumor over the ten animals, then fitted (a) to Eq. [1] and (b) using the empirical parameter Δ_fADC (slope of $D(\omega)$ versus oscillation frequency) used in previous studies (21,22). Fit residuals and coefficients of determination are used to illustrate the accuracy of the two models when depicting the tumor environment.

D_0 and S/V mapping

Parametric maps of D_0 (in $\mu m^2/ms$), S/V (in μm^{-1}) and R^2 were calculated using all OGSE data for each tumor after spatial smoothing. Spearman correlation coefficients were calculated between D_0, S/V, R^2, and the diffusion values calculated at different diffusion times $t = \Delta_{PGSE}$ = 6/9/16/31 ms and oscillation frequencies f_{OGSE} = 65/75/88/100/125/140/160/180/200/225 Hz. Two tailed unpaired Student's t-tests were performed to assess the difference in the mean D_0 and S/V between in vivo (n=10) and ex vivo (n=7) data of the whole tumor ROI, due to potential differences in slice location and thickness (1.5 vs. 0.1 mm for in vivo and ex vivo, respectively).

Linear fits were repeated on successive subsets of the OGSE data (each time omitting the next lowest oscillation frequency) in order to investigate the validity of the Mitra regime under various imaging conditions (in vivo vs. ex vivo, 20°C vs. 37°C). Confidence intervals of the fit estimates D_0 and S/V substantially widened when fitting Eq. [1] to the data obtained at high frequencies only (+160–230% in [100–225] Hz compared to [65–225] Hz). As a result, this analysis was restricted to the ranges [65–225] Hz and [88–225] Hz, and to samples presenting a high coefficient of determination (R^2>0.8). For each condition, a paired Student's t-test was used to assess whether S/V and R^2 remained the same, i.e. the Mitra regime had been reached.

Influence of temperature in ex vivo imaging

Since measurements performed at low oscillation frequencies and at high temperature (higher D_0) are more likely to violate our initial hypotheses regarding the Mitra regime (i.e. negligible diffusion length with respect to the restriction size), temperature was used as an additional tool to investigate the Mitra regime validity, for a given frequency range. The influence of temperature on ex vivo measurement of D_0 and S/V was investigated by comparing two DWI data acquired at room temperature (≈20°C) and subsequently at 37°C on the same day. We hypothesized that D_0 would vary with temperature while S/V would remain constant in the Mitra regime. This hypothesis was tested by using two tailed unpaired Student's t-tests for the mean differences between the DWI data at two different temperatures.

RESULTS

In vivo time dependent diffusion

A representative example of $D(\omega)$ variation with the oscillation frequency $\omega = 2\pi f_{OGSE}$ is illustrated in Fig. 2A. Although the direct comparison of OGSE and PGSE data is flawed due to the imperfect conversion of diffusion times to oscillation frequencies (18), the PGSE

dataset was attributed for visualization purposes an equivalent oscillation frequency $f_{eq} = 1/(4\Delta_{PGSE})$, as in (24).

On a qualitative level, inside each tumor (Fig. 2B), in vivo OGSE $D(\omega)$ measurements (gray area in Fig. 2A) decrease linearly with the inverse square root of ω (R^2>0.9), a hallmark of the Mitra limit. PGSE measurements deviate from the fit of Eq. [1] when the diffusion time Δ_{PGSE} > 6ms. Compared to the tumor, the $D(\omega)$ calculated in the gray matter (GM; Fig. 2A, open circles) showed very little time dependence of $D(\omega)$. The coefficients of determination R^2 in the GM were not considered large enough to support evidence of short-time regime in healthy brain tissue (R^2<0.5).

The diffusion maps calculated inside the tumor (Fig. 2B, white ROI) for various diffusion times and oscillation frequencies can be seen in Fig. 2C–E, along with the S/V, D_0 and R^2 parametric maps derived from voxel-based fitting of Eq. [1] (Fig. 2F–H). Parametric maps revealed very good fitting performances inside the tumor (Fig. 2H), surrounded by lower R^2 values near the edges.

Ex vivo time dependent diffusion

Ex vivo $D(\omega)$ measurements inside the tumor (Fig. 3A, white squares) showed very good agreement with Eq. [1]. As expected, the diffusion in PBS was found larger than that in the tumor and did not vary with diffusion time nor oscillation frequency (Fig. 3A, blue squares). The ex vivo sample surrounded by PBS was mounted between two coverslips (Fig. 3B) and inserted inside the MR histocoil (23) (Fig. 3C–D), leading to comparable SNR values in vivo and ex vivo (120 and 60, respectively) despite a substantial difference in sample thicknesses (1.5 and 0.1 mm, respectively). The final image quality can be assessed based on the b=0 image (Fig. 3B.). Parametric maps (Fig. 3I–K) highlighted good agreement to the Mitra regime. Similar spatial patterns could be observed in diffusion maps (Fig. 3F–H), and S/V and D_0 maps (Fig. 3I–J).

Fit and residuals: S/V versus Δ_fADC

Both fits (to Eq. [1], and using the empirical slope Δ_fADC for the increase of $D(\omega)$ with oscillation frequency) presented high coefficients of determination (R^2=0.98 and 0.93, correspondingly) in vivo at tumor level (Fig. 4A–B, n=10). However, the evidently non-random structure of the Δ_fADC fit residuals (Fig. 4D) suggested that $D(\omega)$ did not increase linearly with the oscillation frequency at a constant rate Δ_fADC. Hence, this empirical model, despite its recent use in (21,22), is not suited to characterize $D(\omega)$ in the range [65–225] Hz. On the other hand, the fit residuals for Eq. [1] (Fig. 4C) are highly random and uncorrelated, which is expected from a physically appropriate model. This allows us to further use the model [1] for quantifying biophysical tissue parameters in the short time limit.

In the Mitra limit, coefficients of determination R^2 applied to in vivo and ex vivo data are presented in Table 1. At ROI level, S/V fits showed good performances for the in vivo (R^2=0.93) and ex vivo (R^2=0.89) data. At voxel level, the R^2 distribution was significantly enhanced by spatial smoothing (+0.25, P<0.05), allowing for more robust voxel-wise analysis and parametric mapping (in vivo / ex vivo: R^2=0.70±0.23 / 0.75±0.20, n=1407 /

1494). Spatial filtering is used throughout the rest of this manuscript. Whole brain parametric mapping revealed very different R^2 distributions in tumor and healthy brain structures (normal brain: R^2=0.22±0.19, n=2921).

Correlation with ADC measures

Table 2 shows the correlation coefficients ρ between S/V, D_0 and conventional DWI metrics - $D(\omega)$ or $D(t)$ at three different frequencies/times as representative examples. S/V did not correlate with $D(t)$ calculated at long diffusion times (ρ<0.7, first two columns). The correlation between S/V and $D(t)$ increased mildly as the diffusion time decreases (supporting Tables S2–3). Ex vivo, S/V was found highly correlated with every $D(\omega)$ metrics in the range [60–200] Hz (0.81 ≤ρ≤0.87, maximum at 65 Hz). In vivo, the correlation between $D(\omega)$ and S/V peaked at 65 Hz (ρ=−0.76) and decreased regularly with f_{OGSE} (ρ= −0.43 for f_{OGSE}=200 Hz).

In vivo and ex vivo ρ between D_0 and $D(\omega)$ generally increased with f_{OGSE}. Ex vivo, D_0 correlated highly with all $D(\omega)$ (ρ≥0.92) and $D(t)$ (ρ≥0.76) metrics. In vivo PGSE measurements were only mildly reflected by D_0 (0.59 ρ≥0.77).

In general, S/V and D_0 were better represented by $D(\omega)$ measured at low & high frequency, respectively. By contrast, the coefficient of determination R^2 corresponding to Eq. [1] was not significantly correlated to any diffusion measurement.

Frequency range for the Mitra regime

S/V ratios were found significantly lower (Fig. 5, −36%, P<0.01) ex vivo at room temperature (0.37±0.05 μm^{-1}) and at 37°C (0.31±0.06 μm^{-1}) than in vivo (0.55±0.06 μm^{-1}). In vivo D_0 values (1.73±0.10 μm^2/ms) were significantly higher (P<0.01) than ex vivo at room temperature (1.39±0.10 μm^2/ms), and lower (P<0.01) than ex vivo at 37°C (1.90±0.14 μm^2/ms).

Temperature decrease was used to determine the adequate range of frequencies for the Mitra regime. Ex vivo, S/V measurements in the range [65–225] Hz were significantly lower (−17%, P<0.05) at 37°C than at room temperature (Fig. 5A, white bars in second/third columns), suggesting the Mitra regime might not be fully reached in that frequency range at 37°C. When fitting the OGSE data in the range [88–225] Hz (gray bars), no significant difference was found between the S/V measured at the two temperatures (gray bars in second/third columns, P=0.40). This implies that S/V measured with an adequate range of short diffusion times (i.e., [88–225] Hz in this study) may be a tissue microstructure related parameter independent of free diffusivity D_0 of the water molecules.

Increasing the lowest oscillation frequency used for fitting was used to ensure better data agreement with Eq. [1]. This translated to a significant S/V increase (gray/white bars) on in vivo (+7%, P<0.01) and ex vivo S/V measurements (+12%, P<0.01) performed at 37°C (Fig. 5A, first/third columns). This had however no significant impact on S/V values based on the ex vivo DWI data acquired at room temperature (second column, P=0.8), suggesting the Mitra regime was already reached in the range [65–225] Hz. In vivo, the S/V measured in

the range [88–225] Hz was significantly (paired t-test, $P< 0.01$) higher than that in the range [65–225] Hz.

A similar observation can also be made with D_0. Increasing the brain sample temperature (from 20°C to 37°C) led to a significant D_0 increase (Fig. 5B, second/third columns, +37%, $P<0.01$), consistent with the relative diffusion increase in PBS (+31%, data not shown). Paired Student's t-tests revealed a small D_0 increase (+2%, $P<0.01$) when increasing the lowest oscillation frequency used to fit the DWI data acquired at 37°C to Eq. [1] (Fig. 5B, first/third columns). This effect was not observed on the ex vivo OGSE data obtained at room temperature (second column, $P=0.7$).

Histology

Figure 6 shows a comparison of S/V map with an adjacent slice stained with GLUT1 and hematoxylin. GLUT1/hematoxylin staining (Fig. 6C–D, blue/brown) depicts a variety of nuclear/cellular sizes, and non stained structures provided a qualitative assessment of the extracellular space (ECS). Based on the DWI data, a 50% S/V decrease was measured between the black and white ROIs delineated in Fig. 6A. On the histology, these two regions (Fig. 6C/D) presented major differences at the micro-structural level, such as variations in nuclear and cell sizes or ECS volume. In this sample, the lowest S/V values (Fig. 6A, white arrow) were also measured near the location of a necrotic area (Fig. 6B, black arrow). These findings are qualitatively consistent with a simple intuition of S/V being inversely proportional to the characteristic length scale between membranes.

DISCUSSION

Our results demonstrate that OGSE diffusion measurements in glioma at moderately high frequencies (65–225 Hz) can be well characterized by a linear relationship between $D(\omega)$ and the inverse square root of the oscillation frequency. Two parameters, free diffusivity D_0 and surface to volume ratio S/V, can be unambiguously derived from this relationship in the very short diffusion time (Mitra) regime.

For simple geometries, such as infinite planes, infinite cylinders or spheres, the dependence of the MR signal on diffusion acquisition parameters and sequences (PGSE/OGSE) can be calculated (27,28). Recent studies have used these geometrical models to investigate the variations of MR signal with various diffusion times and assess the degree of vasculature (29) and the amount of ECS inside various mouse tumors (30). These results are promising, as these metrics can respectively reflect drug delivery efficiency and cell proliferation. However, even in the simplest models the large number of parameters required to model the tumor microenvironment affects the fits robustness, making these studies very sensitive to a priori assumptions or knowledge on the underlying microstructure, which can be very chaotic and/or spatially heterogeneous in the case of aggressive tumors (31). Furthermore, the functional dependence of the diffusivity at low frequency due to disordered arrangement of restrictions is non-analytic, and thereby fundamentally distinct from that in regular geometries (15), making such simplistic models inadequate for quantifying tissue properties whenever the measurements are mostly sensitive to low frequencies or long times (11). On the other hand, here it is shown that the universal high-frequency (Mitra) regime —

following Eq. [1] with only 2 parameters (S/V, D_0) — is an adequate parsimonious way to characterize tumor microstructure, provided it can be reached with existing experimental hardware. In essence, it is shown here that this limit is achievable in brain tumors. In healthy brain tissue, where most water is located within small axons and dendrites (32), this would require frequencies exceeding 1 kHz (11).

The universal model [1] provided more accurate DWI descriptions in our mouse glioma model than via the empirical slope Δ_fADC previously reported (21,22), since the frequency dependence is not really linear, as our fit residuals analysis has shown. Based on our data, Δ_fADC was only mildly correlated with S/V, as both diffusivity and geometrical restrictions are entangled in one parameter. Nevertheless, this parameter could, in absence of strong D_0 variations, reflect S/V changes in a qualitative fashion, rationalizing its empirical correlations useful for tumor treatment follow-up (22) and cellularity mapping (21).

The validity of the Mitra regime depends both on the free diffusivity value, and on the restrictions by the tissue microarchitecture. In particular, diffusion times must be short enough so that only a fraction of the total spin population (close to the membranes) experiences restrictions, while the rest still diffuse freely. In a highly diffusive medium, this translates into even shorter diffusion times to achieve this limit. Therefore, higher oscillation frequencies might be necessary in order to reach the Mitra regime at 37°C inside warm-blooded animals, possibly explaining the small S/V increase when fitting the in vivo DWI data to a reduced range of high oscillation frequencies. Reducing the diffusion time range used for fitting led to a significant increase on the S/V and D_0 confidence intervals, and limited our analysis to the range [65–225] and [88–225] Hz. Although our S/V measurements were consistent for different temperatures, further investigation at higher frequencies would help validate that the Mitra regime was indeed reached at 88 Hz. In this study, frequencies higher than 225 Hz could not be reached while maintaining a reasonable echo time (70ms) and sufficient diffusion contrast (b_{max}=0.4 ms/μm^2) due to hardware constraints (G < 75 G/cm). Interestingly, the criterion of validity (or lack thereof) for the Mitra regime can also be used as a tool to delineate the tumor in the brain, based on the very different distributions of the coefficient of determination R^2 in the tumor and in healthy brain.

Based on room temperature ex vivo DWI data, which we assume fall into the Mitra regime, S/V correlated well with $D(\omega)$ in the range [65–225] Hz. This is encouraging, as OGSE diffusion maps have been used to highlight difference in cellular density (21) that must translate into S/V variations. However, correlations were less pronounced for S/V than for D_0, suggesting as in (33) that $D(\omega)$ is not an exclusive marker for cellular density, as it is also highly dependent on D_0. This observation substantiates that S/V is potentially a better biomarker for cellularity than $D(\omega)$ or $D(t)$, being relatively independent from diffusivity variations introduced by temperature changes in ex vivo samples. This could be of utmost interest in situations subject to diffusivity changes (ischemia, post-injury states) that impact the correlation of conventional diffusion metrics with cellularity (34).

In addition to cellular changes in shape and/or packing, the short-time diffusion regime provides a quantitative estimation of the free diffusivity. This is in itself a very interesting

metric, as D_0 cannot be obtained by conventional methods. In essence, D_0 is obtained via an extrapolation of the observed $D(\omega)$ towards infinite ω, which can only be achieved by knowing the right functional dependence, Eq. [1]. It represents an objective quantitative marker of free water movement, not experiencing mesoscopic restrictions, and independent of the various MRI parameters used to determine it. Inside one voxel, D_0 is likely to represent a weighted average of the various free diffusivities inside each cellular compartment (nucleus/cytoplasm/ECS), and could provide an alternative insight into the content of cells or the extracellular matrix. Further studies are necessary in order to investigate variations of D_0 following tumor treatment and assess its utility in cancer MRI.

Validating the short-time diffusion regime was made possible by using a histocoil (23) allowing for the imaging of very thin brain slices (100 μm) that could adjust quickly to the environmental conditions (multiple temperatures) inside the magnet bore. Another utility of histocoils lies in the possibility to image one (or two neighboring) section(s) using different modalities, using MRI and histology or optical microscopy for instance. Our marker for membrane staining (GLUT1) was not only expressed on the membrane, but labeled equally the cytoplasm and nucleus of this mouse tumor model. This limited our analysis to qualitative comparisons of the S/V estimates with the cell density and ECS volume fraction, both contributing to the resulting surface-to-volume ratio. Although a rigorous quantitative comparison between DWI and histology is not possible without additional assumptions on the shape and packing of the cells, qualitative comparisons support the validity of S/V measurement; low ECS and/or high cell density would increase the total surface-to-volume ratio of restrictions due to membranes, which is compatible with the OGSE-based S/V increase. Future study is warranted to use an exclusive cell membrane staining method to measure S/V from the histology.

The comparison of in vivo and ex vivo tumor samples showed a significant S/V decrease (−36%). This behavior is perhaps counterintuitive, as brain structures and the extracellular matrix are known to shrink under the influences of chemical fixatives (35), which should bring more membranes into a given volume, thereby increasing S/V. Currently, we see the major possible contributing factors to the S/V reduction being (a) partial cellular membrane deterioration or loss of cellular structures (especially near necrotic areas) during fixation and tissue processing; and (b) the reduction of the “apparent” surface area visible with our methodology due to the structural rearrangements (membranes sticking to each other or curving) during tissue fixation. Indeed, the smallest diffusion length scale we can probe (with $f_{max} \approx 200$ Hz) is $L_{\min} \approx \sqrt{D_0 t} \approx \sqrt{D_0 / f_{\max}} \approx 1\,\mu\mathrm{m}$. Effectively, this imposes a low-pass filter on structural details, such that two surfaces that come closer to each other than $L_{\min}$ are seen as one; also, a surface with the curvature radius below $L_{\min}$ does not contribute to the lowest order Mitra correction, as higher-order terms take over in the short-time expansion of $D(t)$ (16). To date, there is no other method to measure S/V for both in vivo and ex vivo cases, hence the question about which of the above factors is dominant in the apparent S/V reduction is left unanswered. Future experiments involving whole brain ex vivo MRI as an additional step will help resolve the question of tissue integrity during sectioning and fixation. Further validation and development of the S/V mapping technique

demonstrated in this study may lead to an effective way to investigate such tissue microstructural changes non-invasively.

The glioma model used in this study was found poorly vascularized between 2 and 4 weeks after tumor cell implantation, in good agreement with GL261 literature (36), suggesting that tumor cells first proliferate near existing vessels, before triggering vascular apoptosis and involution. The angiogenesis necessary for further growth of the GL261 tumor cells only starts 4 weeks after tumor implantation. However, non-negligible IVIM effects have been reported for rat brain gliomas (37). In addition, IVIM was used to identify high-grades (mainly glioblastoma multiforme) from low-grade brain tumors based on the IVIM perfusion fraction distribution (38). In well perfused regions, the diffusion signal would not behave mono-exponentially in the range b=[0–0.4] ms/μm^2. However, our method can also be generalized to the cases with non-negligible IVIM effect by using around 150–200 s/mm^2 as the lower limit of the b-values to minimize the influence from the IVIM effect. A further investigation is warranted for selection of optimal b-values in the presence of non-negligible IVIM effect.

In summary, it is possible to characterize the geometrical restrictions inside a mouse glioma in the very short diffusion time regime using the surface-to-volume ratio, at no cost of additional assumptions for the tumor microenvironment. This provides a quantitative tool to analyze tumor progression or treatment efficacy using MRI. Results can be unambiguously interpreted in terms of geometric changes and/or variations of the diffusive medium. Based on available commercial hardware, ex vivo OGSE DWI performed at room temperature were very well described by S/V and D_0 in the very-short time diffusion regime. Although OGSE studies have only recently started to emerge in clinical research (39,40), these results support the growing interest in time-dependent diffusion in cancer MRI.

Supplementary Material

Refer to Web version on PubMed Central for supplementary material.

Acknowledgments

This work was supported in part by NIH R01CA160620 and was performed under the OCS Small Animal Imaging Core partially funded by the NYU Laura and Isaac Perlmutter Cancer Center Support Grant, NIH/NCI P30CA016087. The Center for Advanced Imaging Innovation and Research (CAI^{2}R, www.cai2r.net) at New York University School of Medicine is supported by NIH/NIBIB P41 EB017183.

References

1. Taouli B, Vilgrain V, Dumont E, Daire JL, Fan B, Menu Y. Evaluation of liver diffusion isotropy and characterization of focal hepatic lesions with two single-shot echo-planar MR imaging sequences: Prospective study in 66 patients. Radiology. 2003; 226(1):71–78. [PubMed: 12511671]
2. Hayashida Y, Yakushiji T, Awai K, Katahira K, Nakayama Y, Shimomura O, Kitajima M, Hirai T, Yamashita Y, Mizuta H. Monitoring therapeutic responses of primary bone tumors by diffusion-weighted image: initial results. Eur Radiol. 2006; 16(12):2637–2643. [PubMed: 16909220]
3. Manenti G, Di Roma M, Mancino S, Bartolucci DA, Palmieri G, Mastrangeli R, Miano R, Squillaci E, Simonetti G. Malignant renal neoplasms: correlation between ADC values and cellularity in diffusion weighted magnetic resonance imaging at 3 T. Radiol Med. 2008; 113(2):199–213. [PubMed: 18386122]

4. Padhani AR, Liu G, Koh DM, Chenevert TL, Thoeny HC, Takahara T, Dzik-Jurasz A, Ross BD, Van Cauteren M, Collins D, Hammoud DA, Rustin GJ, Taouli B, Choyke PL. Diffusion-weighted magnetic resonance imaging as a cancer biomarker: consensus and recommendations. Neoplasia. 2009; 11(2):102–125. [PubMed: 19186405]
5. Kim S, Loevner L, Quon H, Sherman E, Weinstein G, Kilger A, Poptani H. Diffusion-Weighted Magnetic Resonance Imaging for Predicting and Detecting Early Response to Chemoradiation Therapy of Squamous Cell Carcinomas of the Head and Neck. Clin Cancer Res. 2009; 15(3):986–994. [PubMed: 19188170]
6. Niendorf T, Dijkhuizen RM, Norris DG, Campagne MV, Nicolay K. Biexponential diffusion attenuation in various states of brain tissue: Implications for diffusion-weighted imaging. Magn Reson Med. 1996; 36(6):847–857. [PubMed: 8946350]
7. Mulkern RV, Gudbjartsson H, Westin CF, Zengingonul HP, Gartner W, Guttmann CRG, Robertson RL, Kyriakos W, Schwartz R, Holtzman D, Jolesz FA, Maier SE. Multi-component apparent diffusion coefficients in human brain. Nmr Biomed. 1999; 12(1):51–62. [PubMed: 10195330]
8. Kiselev, VG. Ch 10. The Cumulant Expansion: an Overarching Mathematical Framework for Understanding Diffusion NMR. In: Jones, DK., editor. Diffusion MRI: theory, methods and applications. Oxford University Press; New York: 2010.
9. Jensen JH, Helpern JA, Ramani A, Lu HZ, Kaczynski K. Diffusional kurtosis imaging: The quantification of non-Gaussian water diffusion by means of magnetic resonance imaging. Magn Reson Med. 2005; 53(6):1432–1440. [PubMed: 15906300]
10. Novikov DS, Kiselev VG. Effective medium theory of a diffusion-weighted signal. Nmr Biomed. 2010; 23(7):682–697. [PubMed: 20886563]
11. Burcaw LM, Fieremans E, Novikov DS. Mesoscopic structure of neuronal tracts from time-dependent diffusion. NeuroImage. 2015; 114:18–37. [PubMed: 25837598]
12. Portnoy S, Flint JJ, Blackband SJ, Stanisz GJ. Oscillating and Pulsed Gradient Diffusion Magnetic Resonance Microscopy Over an Extended b-Value Range: Implications for the Characterization of Tissue Microstructure. Magn Reson Med. 2013; 69(4):1131–1145. [PubMed: 22576352]
13. Fieremans E, Novikov DS, Jensen JH, Helpern JA. Monte Carlo study of a two-compartment exchange model of diffusion. Nmr Biomed. 2010; 23(7):711–724. [PubMed: 20882537]
14. Novikov DS, Fieremans E, Jensen JH, Helpern JA. Random walk with barriers. Nature physics. 2011; 7(6):508–514. [PubMed: 21686083]
15. Novikov DS, Jensen JH, Helpern JA, Fieremans E. Revealing mesoscopic structural universality with diffusion. P Natl Acad Sci USA. 2014; 111(14):5088–5093.
16. Mitra PP, Sen PN, Schwartz LM. Short-Time Behavior of the Diffusion-Coefficient as a Geometrical Probe of Porous-Media. Phys Rev B. 1993; 47(14):8565–8574.
17. Latour LL, Svoboda K, Mitra PP, Sotak CH. Time-Dependent Diffusion of Water in a Biological Model System. P Natl Acad Sci USA. 1994; 91(4):1229–1233.
18. Novikov DS, Kiselev VG. Surface-to-volume ratio with oscillating gradients. J Magn Reson. 2011; 210(1):141–145. [PubMed: 21393035]
19. Schachter M, Does MD, Anderson AW, Gore JC. Measurements of restricted diffusion using an oscillating gradient spin-echo sequence. J Magn Reson. 2000; 147(2):232–237. [PubMed: 11097814]
20. Xu JZ, Xie JP, Jourquin J, Colvin DC, Does MD, Quaranta V, Gore JC. Influence of Cell Cycle Phase on Apparent Diffusion Coefficient in Synchronized Cells Detected Using Temporal Diffusion Spectroscopy. Magn Reson Med. 2011; 65(4):920–926. [PubMed: 21413058]
21. Aggarwal M, Jones MV, Calabresi PA, Mori S, Zhang JY. Probing mouse brain microstructure using oscillating gradient diffusion MRI. Magn Reson Med. 2012; 67(1):98–109. [PubMed: 21590726]
22. Xu JZ, Li K, Smith RA, Waterton JC, Zhao P, Chen HD, Does MD, Manning HC, Gore JC. Characterizing Tumor Response to Chemotherapy at Various Length Scales Using Temporal Diffusion Spectroscopy. Plos One. 2012; 7(7)
23. Hoang DM, Voura EB, Zhang C, Fakri-Bouchet L, Wadghiri YZ. Evaluation of Coils for Imaging Histological Slides: Signal-to-Noise Ratio and Filling Factor. Magn Reson Med. 2014; 71(5): 1932–1943. [PubMed: 23857590]

24. Parsons EC Jr, Does MD, Gore JC. Temporal diffusion spectroscopy: theory and implementation in restricted systems using oscillating gradients. Magn Reson Med. 2006; 55(1):75–84. [PubMed: 16342147]
25. Kiselev, VG.; Dhital, B. Recipes of Diffusion Measurements with Oscillating Gradients. Proceedings of the ISMRM 22th Annual Meeting and Exhibition; Milan, Italy. 2014; p. 2641
26. Sukstanskii AL. Exact analytical results for ADC with oscillating diffusion sensitizing gradients. J Magn Reson. 2013; 234:135–140. [PubMed: 23876779]
27. Xu JZ, Does MD, Gore JC. Quantitative characterization of tissue microstructure with temporal diffusion spectroscopy. J Magn Reson. 2009; 200(2):189–197. [PubMed: 19616979]
28. Gore JC, Xu JZ, Colvin DC, Yankeelov TE, Parsons EC, Does MD. Characterization of tissue structure at varying length scales using temporal diffusion spectroscopy. Nmr Biomed. 2010; 23(7):745–756. [PubMed: 20677208]
29. Panagiotaki E, Walker-Samuel S, Siow B, Johnson SP, Rajkumar V, Pedley RB, Lythgoe MF, Alexander DC. Noninvasive Quantification of Solid Tumor Microstructure Using VERDICT MRI. Cancer Res. 2014; 74(7):1902–1912. [PubMed: 24491802]
30. Reynaud, O.; Winters, KV.; Hoang, DM.; Wadghiri, YZ.; Novikov, DS.; Kim, SG. In vivo and ex vivo Characterization of Extracellular Space (ECS) in mouse GBM using PGSE and OGSE. Proceedings of the ISMRM 23rd Annual Meeting and Exhibition; Toronto, Ontario, Canada. 2015;
31. Almendro V, Marusyk A, Polyak K. Cellular heterogeneity and molecular evolution in cancer. Annual review of pathology. 2013; 8:277–302.
32. Chklovskii DB, Schikorski T, Stevens CF. Wiring optimization in cortical circuits. Neuron. 2002; 34(3):341–347. [PubMed: 11988166]
33. Arlinghaus LR, Li X, Rahman AR, Welch EB, Xu L, Gore JC, Yankeelov TE. On the relationship between the apparent diffusion coefficient and extravascular extracellular volume fraction in human breast cancer. Magn Reson Imaging. 2011; 29(5):630–638. [PubMed: 21531106]
34. Vorisek I, Hajek M, Tintera J, Nicolay K, Sykova E. Water ADC, extracellular space volume, and tortuosity in the rat cortex after traumatic injury. Magn Reson Med. 2002; 48(6):994–1003. [PubMed: 12465109]
35. Wehrl HF, Bezrukov I, Wiehr S, Lehnhoff M, Fuchs K, Mannheim JG, Quintanilla-Martinez L, Kohlhofer U, Kneilling M, Pichler BJ, Sauter AW. Assessment of murine brain tissue shrinkage caused by different histological fixatives using magnetic resonance and computed tomography imaging. Histology and histopathology. 2014
36. Zagzag D, Amirnovin R, Greco MA, Yee H, Holash J, Wiegand SJ, Zabski S, Yancopoulos GD, Grumet M. Vascular apoptosis and involution in gliomas precede neovascularization: a novel concept for glioma growth and angiogenesis. Laboratory investigation; a journal of technical methods and pathology. 2000; 80(6):837–849.
37. Iima M, Reynaud O, Tsurugizawa T, Ciobanu L, Li JR, Geffroy F, Djemai B, Umehana M, Le Bihan D. Characterization of glioma microcirculation and tissue features using intravoxel incoherent motion magnetic resonance imaging in a rat brain model. Investigative radiology. 2014; 49(7):485–490. [PubMed: 24619211]
38. Federau C, Meuli R, O'Brien K, Maeder P, Hagmann P. Perfusion measurement in brain gliomas with intravoxel incoherent motion MRI. AJNR American journal of neuroradiology. 2014; 35(2): 256–262. [PubMed: 23928134]
39. Baron CA, Beaulieu C. Oscillating gradient spin-echo (OGSE) diffusion tensor imaging of the human brain. Magn Reson Med. 2014; 72(3):726–736. [PubMed: 24142863]
40. Van AT, Holdsworth SJ, Bammer R. In Vivo Investigation of Restricted Diffusion in the Human Brain with Optimized Oscillating Diffusion Gradient Encoding. Magn Reson Med. 2014; 71(1): 83–94. [PubMed: 23447055]

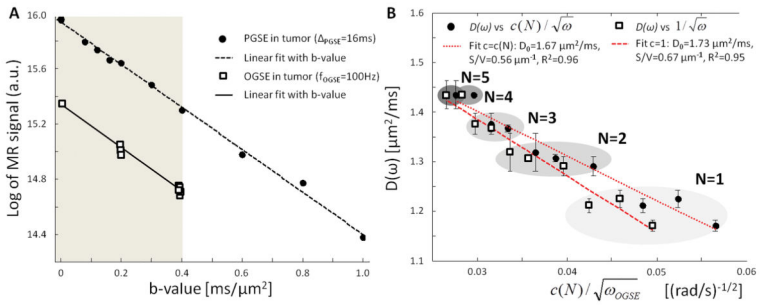

Figure 1. Preliminary studies

A. Inside the glioma, the logarithm of MR signal (black circles) exhibits a linear decrease with b-value in the range [0–0.4] ms/µm^2 (gray area). Near b=0, Intra-Voxel Incoherent Motion effects are negligible compared to the linear fit in the range [0–1] ms/µm^2 (dashed line). OGSE DTI (b=0.2/0.4 ms/µm^2, 3/10 directions, squares) reveals isotropic diffusion inside the glioma. **B.** Impact of correction factor *c(N)* on the linear relationship and *S/V* estimation. Taking into account the correction factor *c(N)* (25) did not significantly improve the coefficient of determination when fitting *D(ω)* (squares/circles) to Eq. [1] (R^2=0.96 for *c(N)* (dotted line) vs R^2=0.95 for *c(N)*=1 (dashed line)). However, assuming *c(N)=1* for $1 \leq N \leq 5$ had a non-negligible impact (+20%) on the *S/V* estimation in the range [65–225] Hz.

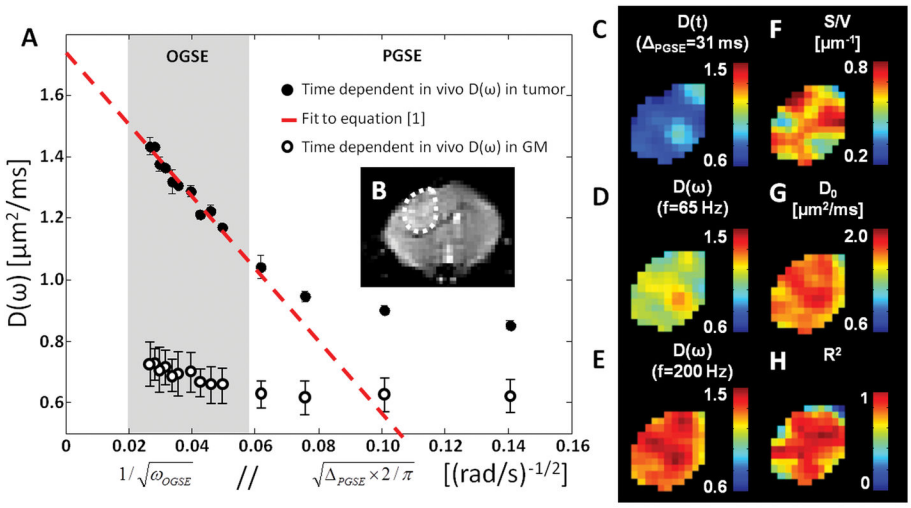

Figure 2. Representative in vivo data

A. Time-dependence of the average $D(\omega)$ in the tumor (black circles) and the GM (open circles) versus inverse square root of oscillation frequency (OGSE, gray box) // square-root of diffusion time (PGSE, white). Error bars represent standard deviations within the ROI. This time dependence becomes asymptotically linear in the high-frequency limit (OGSE). **B.** T2-weighted SE-EPI (b=0, thickness = 1.5 mm) showing tumor location (white ROI) used for parametric mapping. **C**–**E.** Diffusion maps of GL261 obtained at various diffusion times (**C.** Δ_{PGSE} = 31 ms) and oscillation frequencies (**D/E**, f_{OGSE} = 65/200 Hz). **F**–**G.** Maps of the surface-to-volume ratio S/V (F) and of the free diffusivity D_0 (G) inside the glioma. **H.** Map of the coefficient of determination R^2 shows how well Eq. [1] fits to the in vivo OGSE data.

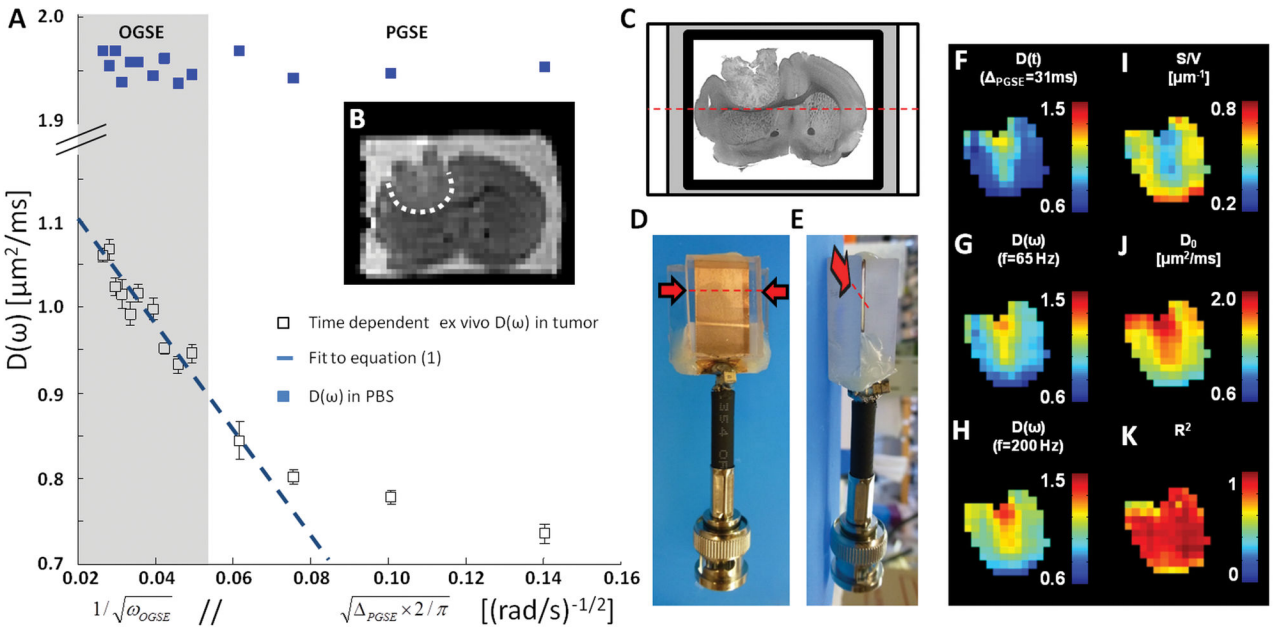

Figure 3. Representative ex vivo data

A. Time-dependence of the average ex vivo $D(\omega)$ in glioma (white open squares) and PBS ROI (blue closed squares) versus inverse square-root of oscillation frequency (OGSE, gray box) // square-root of diffusion time (PGSE, white). Error bars represent standard deviations within the ROI. This time dependence becomes asymptotically linear in the high-frequency limit (OGSE). **B.** T2-weighted SE-EPI (b=0) showing the tumor location (white ROI) inside the brain **C.** An ex vivo sample (thickness = 0.1 mm) immersed in PBS (white) and sealed with Fomblin (gray) is inserted (along dashed red line/arrow) inside a dedicated MR histocoil (**D/E**, lateral/top view). **F–H.** Diffusion maps of GL261 obtained at various diffusion times (**F.** Δ_{PGSE} = 31 ms) and oscillation frequencies (**G/H**, f_{OGSE} = 65/200 Hz). **I–J.** Parametric maps of S/V (I) and free diffusivity D_0 (J) inside the tumor. **K.** Parametric mapping of the coefficient of determination R^2 shows how well Eq. [1] fits to the ex vivo OGSE data.

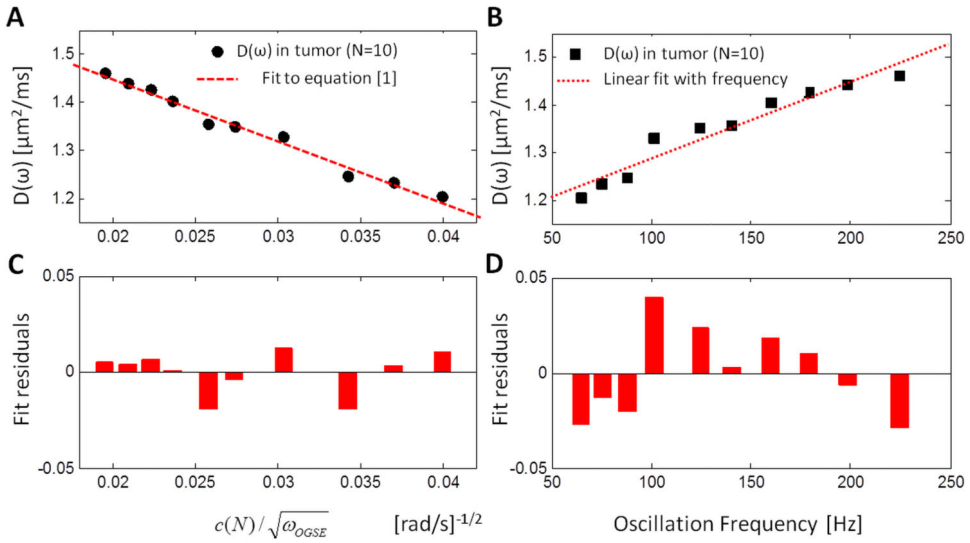

Figure 4. Fitting and fit residuals

Average $D(\omega)$ inside the tumor (circles/squares) and fit (A) to Eq. [1] (dashed line, R^2=0.98) and (B) assuming a linear dependence with the oscillation frequency (dotted line, R^2=0.93). (C) Fit residuals on Eq. [1] highlight randomness of the remaining errors on experimental measurements. (D) Assuming a linear dependence between $D(\omega)$ and the oscillation frequency results in a failure to capture the $D(\omega)$ frequency dependence, illustrated by the temporally correlated fit residuals in the range [65–225] Hz.

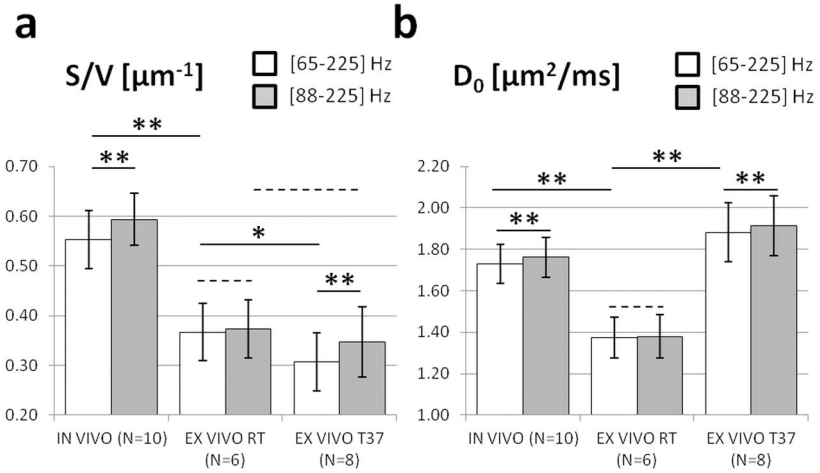

Figure 5. Effect of temperature and oscillation frequency range

on surface-to-volume ratio S/V (A) and free diffusivity D_0 (B), estimated from in vivo (first column, T=37°C) and ex vivo DWI data acquired at room temperature (second column, T=21°C) and 37°C (third column). The gray and white bars represent the mean estimates, in the oscillation frequency range: [65–225] Hz (white), or [88–225] Hz (gray). Error bars represent standard deviations. Statistical significance for a difference between two mean estimates is indicated using an asterisk (P<0.05), double asterisk (P<0.01), or dashed line (P>0.2).

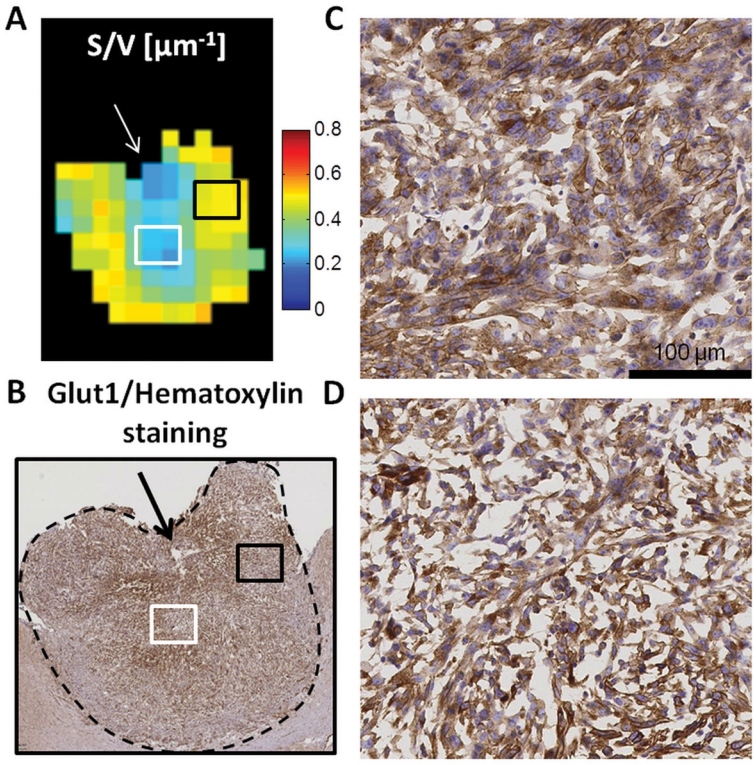

Figure 6. Comparison of DWI data with histology

A. Surface to volume ratio mapping and **B.** GLUT1 (brown) and hematoxylin (blue) staining of GL261 (5 µm thickness). Zooming (x20, scale 100 µm) inside two different regions (**C.** black and **D.** white squares) of the tumor (black dashed line in Fig. 6B) reveals differences in cellular density and size despite non-specific membrane staining. Interestingly, these two regions exhibit different *S/V* values (white/black squares in A.). The white arrow in Fig. 6A indicates a necrotic region that can be seen in Fig. 6B.

Table 1

Coefficients of determination R^2 for equation [1] applied to in vivo and ex vivo $D(\omega)$ data. Ex vivo measurements were performed at room temperature (T=21±1°C).

***S/V* fit**	**GL261 ROI (*n*=10)**	**Single Voxel in GL261**	**Smoothing + Single Voxel in GL261**
R^2 - in vivo	0.93 ± 0.05	0.45 ± 0.28	0.70 ± 0.23
R^2 - ex vivo	0.88 ± 0.06	0.54 ± 0.28	0.75 ± 0.20

Table 2

Spearman correlation coefficients between S/V, D_0, R^2, and various diffusion coefficients for DWI data acquired in the Mitra regime in vivo (n=626) and ex vivo (n=809). Voxels with poor fidelity to equation [1] (R^2<0.8) were not included in this analysis. The highest correlation coefficients for each fitted parameter are indicated in bold. For clarity, only three diffusion metrics are presented here, the complete dataset can be accessed in the supplementary materials.

Fit results	***S/V***		***D_0***		***R^2***	
	In vivo	**Ex vivo**	**In vivo**	**Ex vivo**	**In vivo**	**Ex vivo**
$D(t)_{30ms}$	−0.52	−0.62	0.59	0.76	0.03	−0.22
$D(\omega)_{65Hz}$	**−0.76**	**−0.87**	0.71	0.92	0.12	**−0.23**
$D(\omega)_{200Hz}$	−0.43	−0.84	**0.91**	**0.97**	0.23	−0.19